Journal of Statistical Physics, Vol. 107, Nos. 1/2, April 2002 (© 2002)

Lattice-Boltzmann Simulation of Capillary Rise Dynamics

P. Raiskinmäki,[1, 2] A. Shakib-Manesh,[1] A. Jäsberg,[1] A. Koponen,[1] J. Merikoski,[1] and J. Timonen[1]

Received February 15, 2001; accepted October 21, 2001

We report results of extensive two-phase lattice-Boltzmann simulations of capillary rise dynamics. We demonstrate that the method can be used to model the hydrodynamic behaviour inside a capillary tube provided that the diameter of the tube is large enough, typically at least 30 lattice units. We also present results for the dependence of the cosine of the dynamic contact angle on the capillary number Ca. Its deviation from the static advancing contact angle has a power-law form, with the value of the exponent very close to 3/2 for capillary rise at zero gravity, while behaviour is more complex in the presence of gravity.

KEY WORDS: Lattice-Boltzmann; capillary phenomenon; wetting; two-phase hydrodynamics.

1. INTRODUCTION

Capillary rise, imbibition, droplet spreading and other phenomena related to wetting are of wide theoretical and practical interest.[1–6] While the basic analytical theories have existed for a long time,[7] developments in experimental and computational methods have provided new insights into the fascinating problems involved. One area of such developments is formed by lattice algorithms for fluid dynamics, the lattice-gas models[8–11] and the more recent lattice-Boltzmann models.[12–16] There are now several ways to implement interactions between fluid particles as well as between fluid particles and the environment,[15–22] and the methods have been succesfully tested, e.g., in the contexts of particle suspensions[23] and flow in complex geometries.[8, 17, 24–26]

[1] Department of Physics, University of Jyväskylä, P.O. Box 35, FIN-40351 Jyväskylä, Finland.

[2] To whom correspondence should be addressed; e-mail: Pasi.Raiskinmaki@phys.jyu.fi

0022-4715/02/0400-0143/0 © 2002 Plenum Publishing Corporation

In the present work we consider capillary phenomena and present a simulation model for them. We shall first in Section 2 briefly describe the theoretical hydrodynamical framework, against which we shall compare our results. Relevant technical details of the simulations are given in Section 3. In Sections 4 and 5 we present simulation results for the capillary rise with zero and nonzero gravity. Section 6 comprises a brief discussion of the main implications of our tests on the use of the lattice-Boltzmann method in studies of capillary rise and related phenomena.

2. CAPILLARY PHENOMENON

The simplest example of the capillary phenomenon is naturally the rise of fluid in capillary tube, but the phenomenon also plays an important role when liquid (droplet) penetrates into porous material. Because macroscopic theory of capillary rise is well established, it can provide a useful benchmark test for methods used to simulate imbibition in porous media. In the classical analysis by Washburn,[27] the motion of the incompressible fluid is treated within the assumption of Poiseuille flow[28] (fully developed pipe flow). If the driving force is mainly due to surface tension and gravity force ρg, one can write

$$8\pi\mu(h+h_+)\frac{\mathrm{d}h}{\mathrm{d}t} = 2\pi r\gamma\cos\theta - \pi r^2\rho g h \tag{1}$$

where h is the height of the column measured from the level of the liquid surface outside the tube, h_+ is the length of the part of the capillary tube immersed in the liquid, and r is the radius of the tube with a circular cross section. Fluid density, viscosity, surface tension and contact angle are denoted by ρ, μ, γ and θ, respectively. Including inertial and entrance effects, Eq. (1) becomes

$$\rho h\frac{\mathrm{d}^2h}{\mathrm{d}t^2} + \frac{8\mu(h+h_+)}{r^2}\frac{\mathrm{d}h}{\mathrm{d}t} + \frac{1}{4}\rho\left(\frac{\mathrm{d}h}{\mathrm{d}t}\right)^2 + \rho g h = \frac{2\gamma\cos\theta}{r} \tag{2}$$

Inertial forces can usually be ignored in the overdamped limit $r < r_c = (32\mu^2\gamma\cos\theta/\rho^3 g^2)^{1/5}$.[29]

A further phenomenological correction to Eqs. (1)–(2) involves recognition that θ is not constant, but varies with velocity, which leads to the concept of the (velocity-dependent) dynamic contact angle θ_d.[30] This means also that the dynamics of the fluid in the immediate vicinity of the moving contact line can no more be ignored, which is a real challenge for theoretical and computational models. A number of empirical relationships

for wetting have been discussed in the literature, all of which express the dynamic contact angle θ_d as a function of the capillary number $\mathrm{Ca} = v\mu/\gamma$ during spreading such that $\theta_d = f(\mathrm{Ca}, \theta_a)$, where the advancing contact angle θ_a is that of a spreading liquid in the limit $v \to 0^+$. We shall adopt the expression generally used in studies of capillary rise,[29]

$$\cos\theta_a - \cos\theta_d = A\,\mathrm{Ca}^B \tag{3}$$

where A and B are constants.

In the presence of pinning due to quenched disorder such as chemical impurities or surface roughness, there is an immediate connection with dynamical critical phenomena,[29] because the velocity of the interface behaves as $v = v_0(F/F_c - 1)^\beta$. Hence $\beta = 1/B$ provided that pinning is the dominant mechanism determining the exponent B in Eq. (3). Critical dynamics of contact line depinning has been studied, e.g., in ref. 31 using renormalization group, with the result $\beta \approx 2/3$ for one specific model (for an overview of this and other theoretical results, see ref. 29). We stress that there is no quenched disorder present in our simulations, however.

3. SIMULATION MODEL

In the lattice-Boltzmann method one solves the Boltzmann equation on a regular lattice, where fluid flow is modelled by particle distributions. Of the different lattice-Boltzmann models we use the so-called lattice-BGK (lattice-Bhatnagar–Gross–Krook) algorithm with the D3Q19 lattice.[14] The dynamics of the distribution $f_i(\mathbf{r}, t)$ of particles moving in direction i at a lattice point $\mathbf{r}$ is described by the discrete Boltzmann equation, with the usual choice of the equilibrium distribution (see, e.g., ref. 14).

To model surface tension forces through a nearest and next-nearest neighbour potential, we have adopted the method developed by Shan and Chen.[17–19] In addition to the local collisions, neighbouring fluid particles exchange momentum through the attractive short-range force

$$\mathbf{F}_G(\mathbf{r}) = -\tau\psi(\mathbf{r}) \sum_i G_i \psi(\mathbf{r} + \mathbf{c}_i)\,\mathbf{c}_i \tag{4}$$

where $\psi(\mathbf{r}) = 1 - \exp[-\rho(\mathbf{r})]$ with the total particle density $\rho(\mathbf{r}, t) = \sum_i f_i(\mathbf{r}, t)$, and $G_i = 2G, G, 0$ for the displacement vectors $\mathbf{c}_i$ of length $|\mathbf{c}_i| = 1, \sqrt{2}, 0$ (in lattice units), respectively. The parameter $G < 0$ thus controls the surface tension.

In our simulations the no-slip boundary condition at solid-fluid interfaces is realized through the computationally efficient bounce-back condition,[8]

where the momenta of the particles meeting the solid wall are reversed. Adhesive forces between the fluid and solid phases are introduced via[17]

$$\mathbf{F}_W(\mathbf{r}) = -\tau\psi(\mathbf{r}) \sum_i W_i s(\mathbf{r}+\mathbf{c}_i)\, \mathbf{c}_i \tag{5}$$

where $W_i = 2W, W, 0$ for $|\mathbf{c}_i| = 1, \sqrt{2}, 0$, respectively, and $s = 0, 1$ for fluid and solid, respectively. The interaction strength W is positive for nonwetting fluid and negative for wetting fluid. With these definitions the surface tension force $\mathbf{F}_G$ and the adhesive force $\mathbf{F}_W$ change the momenta of fluid particles at each time step according to[17]

$$\rho(\mathbf{r})\, \mathbf{u}(\mathbf{r}) \to \rho(\mathbf{r})\, \mathbf{u}(\mathbf{r}) + \mathbf{F}_G(\mathbf{r}) + \mathbf{F}_W(\mathbf{r}) \tag{6}$$

We have tested our implementation of this algorithm in the context of droplet spreading in our earlier work,[26] our results there being consistent with those by Martys and Chen in ref. 17.

For the present work we have added the capillary tube as seen in the three snapshots of Fig. 1. The boundary conditions of the three-dimensional simulation domain are fully periodic except for the solid wall at the bottom. The simulations reported below were performed for the tube radii $r = 2, 5, 10, 20$ lattice units. The full domain size was $50 \times 50 \times 200$ for $r = 2, 5, 10$ and $100 \times 100 \times 300$ for $r = 20$. Before the actual capillary simulation we iterated the system without the tube until an equilibrium state with no mass transfer between liquid and gas phases was reached. After this the simulation was continued with the full geometry including the tube. In all simulations reported below the relaxation parameter τ was set to 1. Unless stated otherwise, the adhesion and surface tension parameters have the values $W = -0.1$ and $G = -0.15$, respectively. This results in the density ratio of about 20 between the liquid and the vapour phase, the bulk density of the liquid phase was $\rho = 2.25$, viscosity was $\mu = 0.375$, and the surface tension was $\gamma = 0.085$. By varying the adhesive force, the radius of the tube and gravity, i.e., the paramaters W, r, and g, we were then able to compare the simulation results with numerical solution of Eq. (2).

To present our simulation results in dimensionless units, we define the characteristic time and height as $t_0 = \mu^3/\rho\gamma^2$ and $h_0 = \mu^2/\rho\gamma$, respectively. In the presence of gravity we can also define the dimensionless parameter $\tilde{g} = \mu^4 g/\rho\gamma^3$.

4. SIMULATIONS OF CAPILLARY RISE WITHOUT GRAVITY

In Fig. 2 we present the main result of our capillary simulations at zero gravity, the height of the column as a function of time for four values

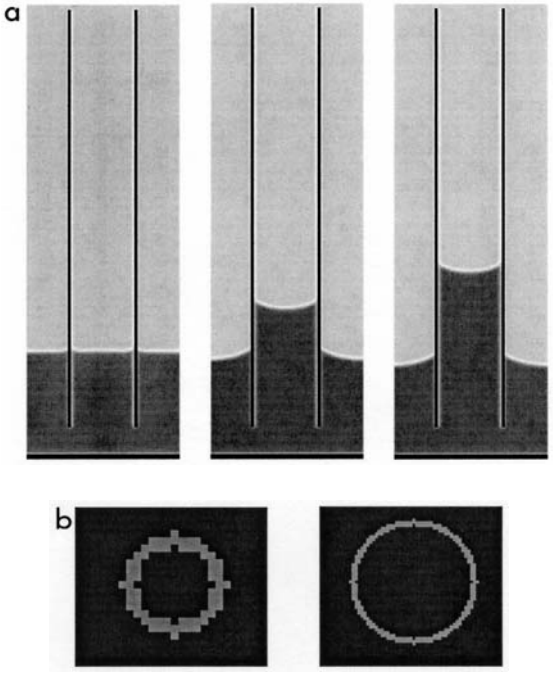

Fig. 1. (a) Three snapshots from a three-dimensional capillary rise simulation with $r = 20$ lattice units: initial, intermediate, and steady state (side view). (b) Discretization of the circular tube for $r = 5$ and $r = 20$ lattice units (top view).

of tube radius with $W = -0.1$ kept constant. Throughout this work we determine the height of the column or the location of the gas-liquid interface as the turning point of a least-squares fit by a tanh function of the density profile in vertical direction. With increasing the tube radius, the column rises faster, as expected. The solid lines in the figure show the corresponding numerical solutions of Eq. (2), where the dynamic contact angle θ_d, defined via Eq. (3), was determined using Eq. (8) as explained below, for $r = 5$, 10, and 20. By using a constant value for θ a satisfactory agreement between Eq. (2) and the simulation data can only be obtained for a short time window up to $t/t_0 \approx 1000$, while by using θ_d an excellent agreement is seen for large r up to the latest data points, the deviation there resulting from an increase in the interface velocity close to the end of the tube.

As expected, the value $r = 2$ is too small for any sensible result. The adhesive force defined through Eq. (5) generates a roughly one lattice unit thick liquid layer on the tube surface. As a result we observe for $r = 2$ a rise

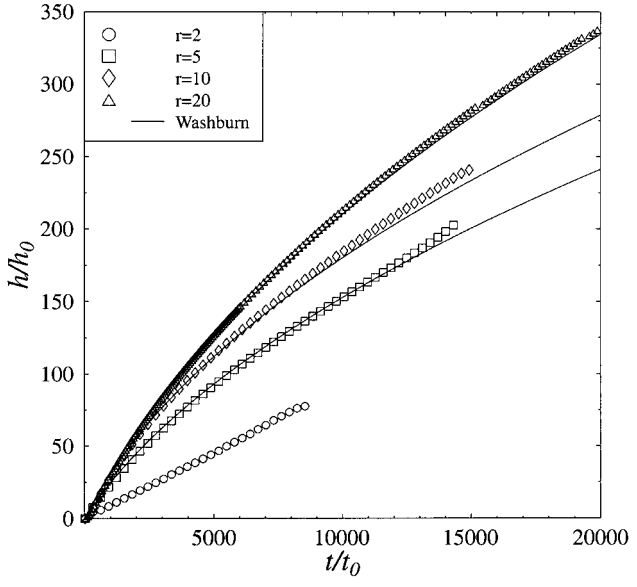

Fig. 2. The height of the fluid column as a function of time for $r = 2, 5, 10, 20$ lattice units. The numerical solutions of the Washburn equation are also presented.

linear in time, and also capillary condensation. For $r = 2$ we actually do not observe bulk liquid density inside the tube at all, as seen in the density profiles of Fig. 3, again for $W = -0.1$. On the outer surface of the tube the density of the vapour is slightly higher than the bulk density of the vapour. Inside the tube the decay of the density close to the wall is similar for $r = 5, 10, 20$, and the proportion of the liquid with bulk density decreases with decrasing radius. With increasing adhesion the density of the fluid at the wall increases, e.g., from 1.5 to 2.0 at the first layer for W going from -0.10 to -0.12, but the range of wall effect in the density is the same.

Due to a rather rough discretization (see also ref. 26), and the density variation shown in Fig. 3, it is impossible, especially for small r, to accurately measure θ_d directly from the density field. For an indirect determination of θ_d, we first apply the one-dimensional Reynolds transport theorem for a control volume to estimate the rate of change of momentum of the system. The upper control surface moves with the meniscus of the liquid column (no outflow from the control volume) and the lower control surface is fixed at the lower end of the tube. Then the rate of change of the total momentum inside the control volume is

$$\frac{\mathrm{d}}{\mathrm{d}t}(m\mathbf{v})_{\mathrm{syst}} = \frac{\mathrm{d}}{\mathrm{d}t}\left[\int_{CV} \mathbf{v}\rho \,\mathrm{d}V\right] + \int_{CS} \mathbf{v}\rho(v_r \cdot \mathbf{n}) \,\mathrm{d}A \tag{7}$$

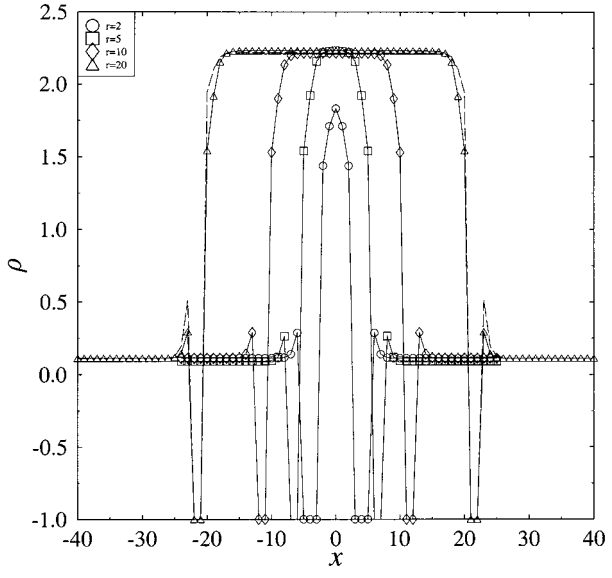

Fig. 3. The density profile across the capillary tube for radius 2, 5, 10 and 20. The dashed line for $r = 20$ shows the profile for stronger adhesion. A negative value of the density indicates the tube wall.

where $m = m(t)$ is the total mass of the fluid inside the control volume, $\mathbf{v}$ is the fluid velocity, and CV and CS denote the volume and surface area of the control volume, respectively. Assuming a constant velocity through the tube we obtain from Eq. (7) for θ_d the expression

$$\cos\theta_d = \frac{1}{2\pi r\gamma}\left[\frac{\mathrm{d}(mv)_{\mathrm{syst}}}{\mathrm{d}t} - v(2\pi r^2\rho v) + 8\pi\mu(h+h_+)\,v + \frac{1}{4}\pi r^2\rho v^2 + \pi r^2\rho g h\right] \tag{8}$$

The second term on the right side of this equation describes the momentum carried by the incoming fluid (at the inlet). We note that the determination of θ_d via Eq. (8) using $h = h(t)$ from the simulation, does not take into account, e.g., the effects of fluid flow near the wall of the tube immediately behind the meniscus, or the displacement of vapour by the liquid. Also, the length h_+ is not strictly constant during the rise due to the absence of sources in the system.

In Fig. 4 we show the behaviour of the dynamic contact angle as a function of the capillary number Ca, which is essentially the interface velocity, again for $W = -0.1$. At the beginning of the simulations $\cos\theta_d = 0$ or $\theta_d = \pi/2$. After this the contact angle θ_d decreases with decreasing Ca.

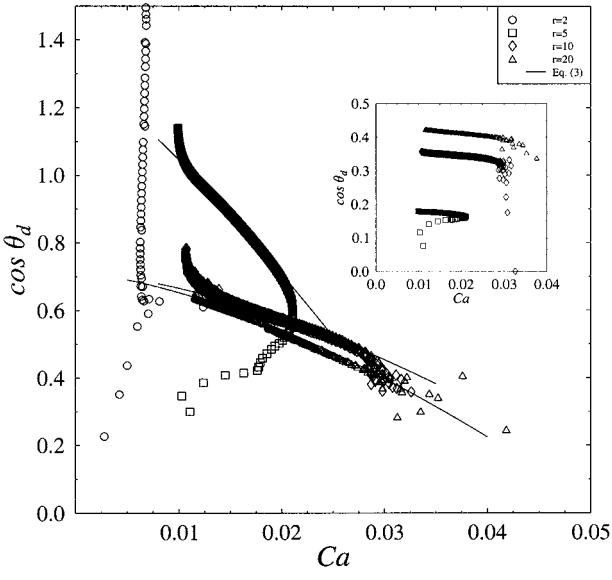

Fig. 4. The dynamic contact angle as a function of Ca for $r = 2, 5, 10, 20$ as detetermined using Eq. (8). Inset: the dynamic contact angle determined directly from the density profile data.

The maximum of Ca is reached very rapidly, in few hundred time steps of the total simulation time of about 50000 time steps. For $r = 5, 10, 20$, the dynamic contact angle follows Eq. (3), if $\cos\theta_a$, A and B are treated as free fitting parameters. In all simulations at zero gravity we find $A = 70$. The results of the fits are summarized in Table I. For the parameter B we obtain $B \approx 3/2$. This value happens to be comparable with some theoretical predictions for contact line dynamics near the pinning threshold (see the end of Section 2).

Table I. Results of the Fits with Eq. (3) for Zero Gravity

r	W	$\mathrm{Ca}_{\max}$	$\cos\theta_a$	A	B
5	−0.10	0.021	1.3	70	1.22
10	−0.10	0.031	0.71	70	1.59
10	−0.11	0.043	1.05	70	1.53
10	−0.12	0.051	1.48	70	1.41
20	−0.10	0.042	0.71	70	1.53

Values $\cos\theta_d > 1$ are clearly unphysical. For comparison we show also the results of the direct determination of $\cos\theta_d$ in the inset of Fig. 4. In the control volume method used to calculate θ_d, the role of the resistive forces is crucial. One source of error is evident from Fig. 5, where we show the velocity profile of a steady flow of the liquid in its equilibrium density between two infite (by using periodic boundary conditions in the simulation) parallel plates. Here there is no phase separation in our two-phase model and the flow is produced by a constant body force at each lattice point. For comparison, we show in Fig. 5 also the result for the single-phase model. A comparison with the well-known analytical results[28] denoted by full curves, shows that the velocity profile has the correct (Poiseuille) parabolic shape, but is shifted. As expected, the relative deviation decreases for increasing r. For stronger adhesion the simulated velocity profile approaches the theoretical curve and boundary effects in the density profile decrease (see Fig. 3), but, on the other hand, at the same time the discrete-lattice effects at the gas-solid interface increase, and values of $\cos\theta_d$ greater than unity are still obtained for small r.

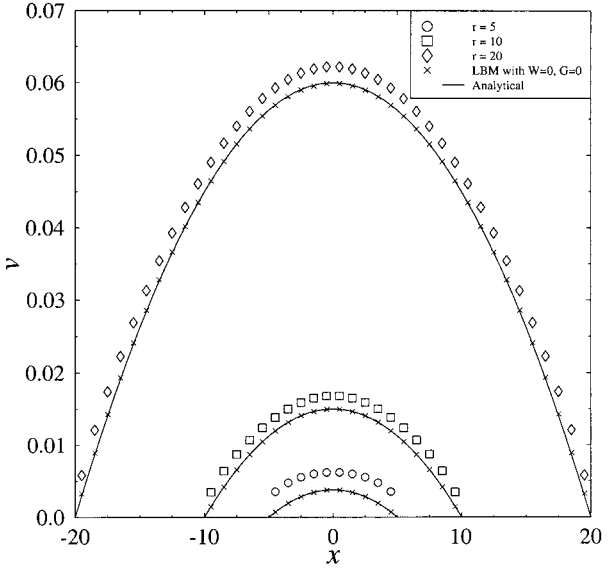

Fig. 5. A typical example of the velocity profile of a fully developed flow of the liquid between two parallel plates: Open symbols show our simulation results for $W = -0.1$, $G = -0.15$, $g = 0$, and the full curves are the analytical expression. For comparison we also show by crosses simulation data for the single-phase model or the case $W = G = g = 0$.

However, for $r = 10, 20$, the results are consistent to the extent that we observe behaviour in the hydrodynamic scale at least for $r = 20$. The biggest uncertainty is related to the discrepancy between the control volume method and the direct determination of θ_d. Note that one cannot use lattice points close to the tube wall so the value of the contact angle obtained using the direct method is too big. For increasing system size and also in the presence of gravity (see next section) the situation gets better. We also note that the increase of $\cos\theta_d$ at small Ca is a result of reaching the end of the tube.

In Figs. 6 and 7 the radius is kept constant, $r = 10$, and adhesion is varied. Again we observe a nice agreement with Eq. (2) and the fitting parameters $A, B, \cos\theta_a$ can be found in Table I. We observe that for stronger adhesion, the trend is to have more finite-lattice problems that otherwise only appear for narrower tubes. Apparently, $r = 10$ is too small for $W = -0.12$, while for $W = -0.10$ it seems to be the smallest reasonable value that can be used. However, even for $W = -0.10$ the value of $\cos\theta_d$ obtained by using Eq. (8) in the limit of small capillary number is quite high compared with the rough (because of discretization) estimate obtained directly from the density profile (inset of Fig. 7).

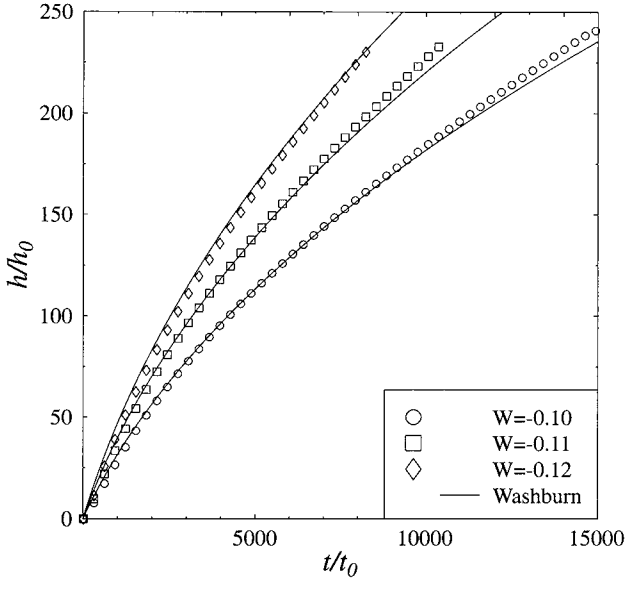

Fig. 6. The height of the fluid column as a function of time for three adhesion strengths $W = -0.10, -0.11, -0.12$, with $r = 10$. The numerical solutions of the Washburn equation are shown by full curves.

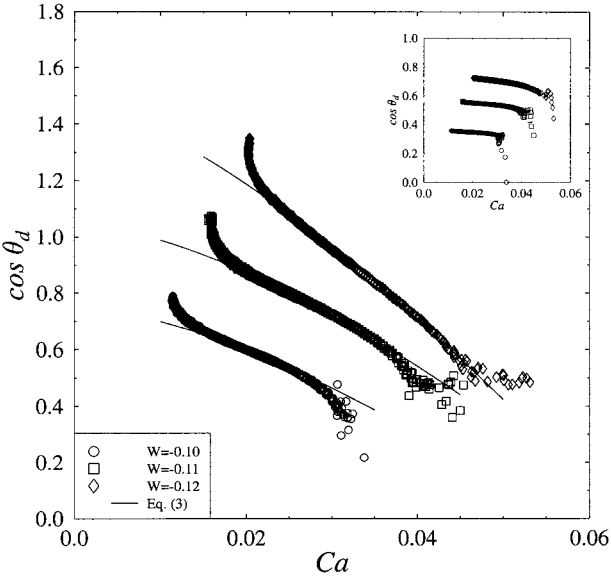

Fig. 7. The dynamic contact angle as a function of Ca for $r = 10$ with three different adhesion strengths $W = -0.10, -0.11$ and -0.12. The numeric result from Eq. (3) is shown by the full curves. Inset: the dynamic contact angle determined directly from the density profile data.

5. SIMULATIONS OF CAPILLARY RISE WITH GRAVITY

We can now add the effect of gravity in the simulation. For the other parameters we use the same values as in the previous section. The simulation results shown in Figs. 8 and 9 agree well with the one obtained from the Washburn equation, in this case also with a constant value of the contact angle for small capillary numbers. Even in plots (not shown) of $h = h(t)$ for $r = 5$, with otherwise the same parameters as in Fig. 9, a reasonable agreement with the theoretical prediction is found.

In Fig. 10 we show $\cos\theta_d$ as a function of Ca. For strong adhesion, the radius $r = 5$ is certainly too small. For small capillary numbers or slow interface velocity, θ_d expectedly becomes constant. Finally, we show in Table II the values of the maximum capillary number from each simulation, the parameters A and B in Eq. (3), and the contact angle θ_{eq} in the final equilibrium state from Eq. (2).

For increasing gravity the relative importance of other resistive forces in Eq. (8) diminishes. It is evident from Figs. 7 and 10 that for increasing gravity there are less problems in the behavior of $\cos\theta_d$. This supports our suggestion above that the frictional forces in our simulation model differ from those assumed in the hydrodynamical derivation of Eq. (8).

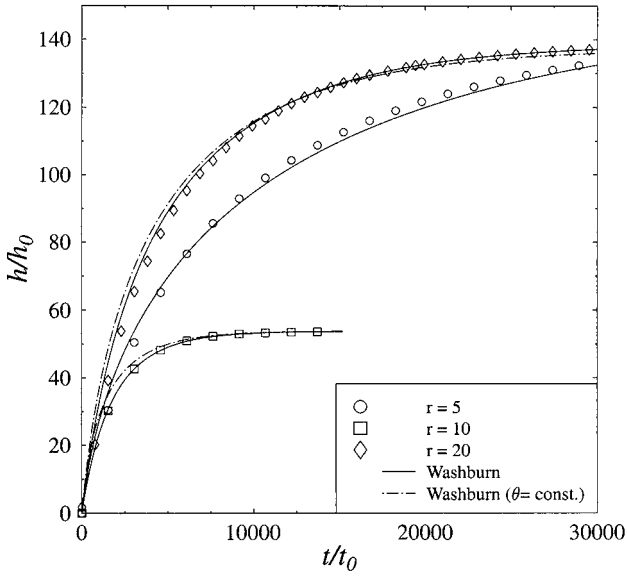

Fig. 8. The height vs. time for $r = 5, 10$ with gravity $\tilde{g} = 0.00146$ and $r = 20$ with gravity $\tilde{g} = 0.000275$.

Table II. Equilibrium Contact Angles and Other Parameters in the Presence of Gravity

r	W	$\tilde{g}$	Ca_{max}	$\cos\theta_{eq}$	A	B
	−0.10		0.026	0.73	1000	2.18
5	−0.11	0.00146	0.033	1.02	1000	2.11
	−0.12		0.040	1.6	155	1.49
	−0.10		0.030	0.50	1000	2.40
10	−0.11	0.00146	0.042	0.71	1000	2.33
	−0.12		0.052	0.89	1000	2.45
	−0.10		0.020	0.61	1000	2.15
5	−0.11	0.008	0.030	0.87	1000	2.08
	−0.12		0.036	1.12	37	1.31
	−0.10		0.023	0.44	6.0	1.0
10	−0.11	0.008	0.032	0.62	7.0	1.0
	−0.12		0.039	0.77	8.5	1.0
20	−0.10	0.000275	0.033	0.51	70	1.75

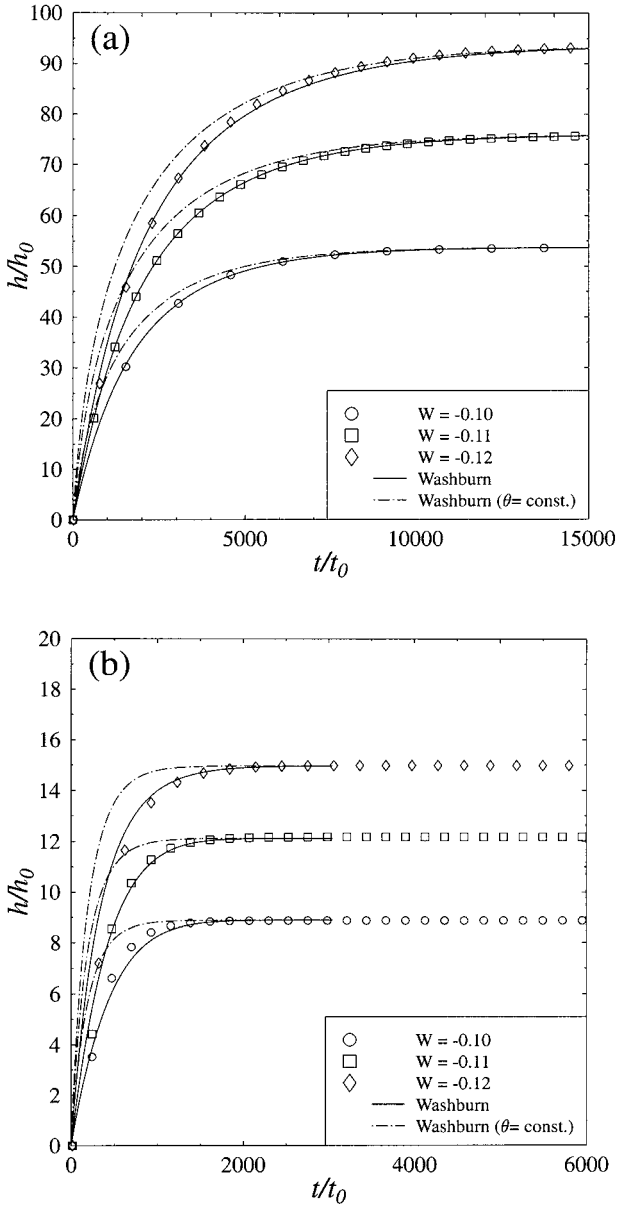

Fig. 9. The height vs. time for $r = 10$ for the adhesive force $W = -0.10, -0.11, -0.12$ with (a) $\tilde{g} = 0.00146$ and (b) $\tilde{g} = 0.008$.

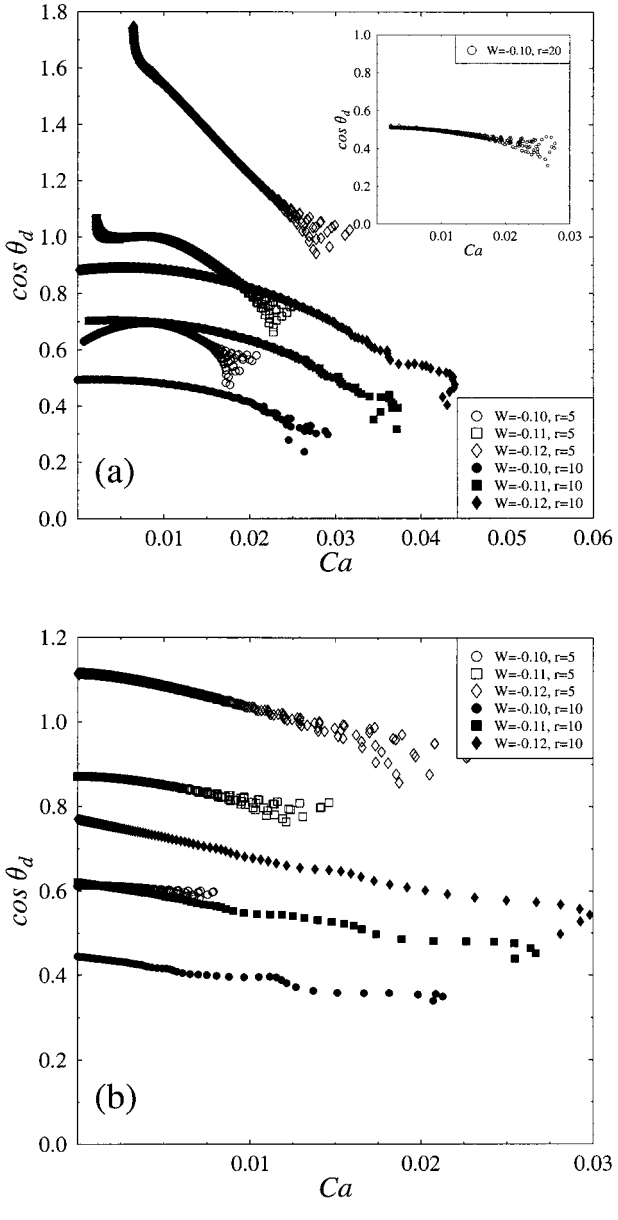

Fig. 10. The dynamic contact angle vs. Ca for $r = 5, 10$ with $W = -0.10, -0.11$ and -0.12. (a) $\tilde{g} = 0.00146$. Inset: The dynamic contact angle for radius $r = 20$ with $W = -0.10$ and $\tilde{g} = 0.000275$. (b) $\tilde{g} = 0.008$.

6. CONCLUSIONS

In this work we have tested the use of the lattice-Boltzmann method in studies of capillary rise. One motivation for such a study is to investigate the possibility to use the method to model imbibition of fluid in porous media. The results are promising: The capillary phenomenon can indeed be studied at the hydrodynamic level. However, it turns out that due to problems related to discretization, one would need rather thick (in lattice units) tubes to get realistic kinetics for the fluid column inside. This is particularly evident from the analysis of our simulation data by using the hydrodynamic description of Eq. (8). With the parametrization used in our studies, the diameter of the tube should be at least 30 lattice units. For static properties our simulations in the presence of gravity indicate that somewhat thinner tubes can be appropriate, while for stronger adhesion thicker tubes are needed. Thus in any reasonable lattice-Boltzman model for two-phase flow in porous media, simulation cells of a size of a several hundred lattice units would be needed in each direction. A challenging question yet to be addressed by simulations, is the role of quenched disorder present in the surfaces of pipes or pores. We hope that the present work can provide a useful benchmark for the construction of such models.

REFERENCES

1. S. A. Safran, *Statistical Thermodynamics of Surfaces, Interfaces, and Membranes* (Addison–Wesley, Reading, 1994).
2. L. H. Tanner, *J. Phys. D: Appl. Phys.* **12**:1473 (1979).
3. M. Pasandideh-fard, Y. M. Qiao, S. Chandra, and J. Mostaghimi, *Phys. Fluids* **8**:650 (1996).
4. T. Mao, D. C. S. Kuhn, and H. Tran, *J. of Pulp and Paper Sci.* **23**:J565 (1997).
5. C. Trevino, F. Mendez, and C. Ferro-Fontan, *Phys. Rev. E* **58**:4473 (1998).
6. S. Betelu, B. M. Law, and C. C. Huang, *Phys. Rev. E* **59**:6699 (1999).
7. For a recent overview and references, see M. Dube, M. Rost, and M. Alava, *Eur. Phys. J. B* **15**:691 (2000).
8. D. H. Rothman and S. Zaleski, *Lattice-Gas Cellular Automata* (Cambridge University Press, Cambridge, 1997).
9. D. H. Rothman, *J. Geophysical Research* **95**:8663 (1990).
10. V. Pot, C. Appert, A. Melayah, D. H. Rothman, and S. Zaleski, *J. Phys. II France* **6**:1517 (1996).
11. U. Frisch, D. d'Humières, B. Hasslacher, P. Lallemand, Y. Pomeau, and J.-P. Rivet, *Complex Syst.* **1**:649 (1987).
12. S. Chen and G. D. Doolen, *Annu. Rev. Fluid Mech.* **30**:329 (1998).
13. G. McNamara and G. Zanetti, *Phys. Rev. Lett.* **61**:2332 (1988).
14. Y. H. Qian, D. d'Humières, and P. Lallemand, *Europhys. Lett.* **17**:479 (1992).
15. A. K. Gunstensen, D. H. Rothman, S. Zaleski, and G. Zanetti, *Phys. Rev. A* **43**:4320 (1991).
16. A. K. Gunstensen and D. H. Rothman, *Europhys. Lett.* **18**:157 (1992).

17. N. S. Martys and H. Chen, *Phys. Rev. E* **53**:743 (1996).
18. X. Shan and H. Chen, *Phys. Rev. E* **47**:1815 (1993).
19. X. Shan and H. Chen, *Phys. Rev. E* **49**:2941 (1994).
20. E. Orlandini, M. R. Swift, and J. M. Yeomans, *Europhys. Lett.* **32**:463 (1995).
21. M. R. Swift, E. Orlandini, W. R. Osborn, and J. M. Yeomans, *Phys. Rev. E* **54**:5041 (1996).
22. G. Gonnella, E. Orlandini, and J. M. Yeomans, *Phys. Rev. E* **58**:480 (1998).
23. A. J. C. Ladd, *J. Fluid. Mech.* **271**, 285 (1994); ibid. **271**, 311 (1994); A. J. C. Ladd and R. Verberg, *J. Statist. Phys.* **104**, 1191 (2001).
24. A. Koponen, D. Kandhai, E. Hellén, M. Alava, A. Hoekstra, M. Kataja, K. Niskanen, P. Sloot, and J. Timonen, *Phys. Rev. Lett.* **80**:716 (1998).
25. B. Ferrèol and D. H. Rothman, *Transport in Porous Media* **20**:3 (1995).
26. P. Raiskinmäki, A. Koponen, J. Merikoski, and J. Timonen, *Comp. Mat. Sci.* **18**:7 (2000).
27. E. W. Washburn, *Phys. Rev.* **17**:273 (1921).
28. F. M. White, *Fluid Mechanics* (McGraw–Hill, New York, 1994).
29. E. Schäffer, and P. Wong, *Phys. Rev. E* **61**:5257 (2000).
30. E. B. Dussan, *Ann. Rev. Fluid Mech.* **11**:371 (1979).
31. D. Ertas, and M. Kardar, *Phys. Rev. E* **49**:R2532 (1994).